ISSN 1063-7826, Semiconductors, 2021, Vol. 55, No. 1, pp. 44–50. © Pleiades Publishing, Ltd., 2021.
Russian Text © The Author(s), 2021, published in Fizika i Tekhnika Poluprovodnikov, 2021, Vol. 55, No. 1, pp. 34–40.

SEMICONDUCTOR STRUCTURES, LOW-DIMENSIONAL SYSTEMS, AND QUANTUM PHENOMENA

Spectroscopic Studies of Integrated GaAs/Si Heterostructures

P. V. Seredin[a,b,*], D. L. Goloshchapov[a], I. N. Arsentyev[c,], D. N. Nikolaev[c], N. A. Pikhtin[c], and S. O. Slipchenko[c]**

[a] *Voronezh State University, Voronezh, 394018 Russia*
[b] *Ural Federal University, Yekaterinburg, 620002 Russia*
[c] *Ioffe Institute, St. Petersburg, 194021 Russia*
**e-mail: paul@phys.vsu.ru*
***e-mail: arsentyev@mail.ioffe.ru*

Received September 3, 2020; revised September 10, 2020; accepted September 10, 2020

Abstract—The purpose of the study is to investigate the effect of a new type of compliant substrates based on an AlGaAs superstructure layer (SL) and a protoporous Si (proto-Si) layer formed on a crystalline Si (*c*-Si) layer on the optical properties of an epitaxial GaAs layer grown by metal–organic chemical vapor deposition. It is for the first time shown that the low-temperature growth of high-quality epitaxial GaAs films can be conducted using SL/proto-Si compliant substrates. The introduction of a SL layer in addition to proto-Si into the composition of the compliant substrate makes it possible to mitigate a number of negative effects of low-temperature growth, to reduce the level of strains in the epitaxial layer, to protect it from self-doping with Si atoms, to reduce the number of technological operations of the growth of transition buffer layers, to improve the structural and morphological characteristics of the epitaxial layer, and to attain good optical characteristics of the layer. The GaAs/Si heterostructures are studied by Raman spectroscopy, photoluminescence measurements, and optical transmission–reflection spectroscopy. The data will serve as an important material for understanding the fundamentals of the physics and technology of integrated III–V/Si heterostructures and for facilitating their use in optoelectronic devices.

Keywords: GaAs/Si heterostructure, compliant substrate, proto-Si, superstructure layer, Raman spectroscopy, photoluminescence, optical spectra

DOI: 10.1134/S1063782621010139

1. INTRODUCTION

The combination of III–V compounds, such as semiconductors of the GaAs group, with silicon substrates presents a unique opportunity for bringing together the benefits of advanced semiconductor materials with the capabilities developed by silicon technology. As a result, this will allow the creation of high-speed and high-power optoelectronic devices, solar cells, light-emitting diodes, lasers, etc. [1–3].

In a number of earlier studies [4–7], we showed that the use of a compliant substrate composed of a nanoporous Si transition layer formed directly on single-crystal silicon (*c*-Si) by electrochemical etching offered considerable promise for the production of GeAs/Si hybrid heterostructures with high functional characteristics. The use of a protoporous Si/Si (proto-Si/Si) compliant substrate allows one to attain the unique optical and electrical characteristics of hybrid III–V/proto-Si/Si heteroepitaxial structures, in which the best transport and optical characteristics of dissimilar materials are combined within one device, and as a result, to cut the cost of finished devices by reducing the number of additional technological processes.

One more technological approach to the production of compliant substrates of a new type can be the introduction of III–V superstructure layers (SL) into the composition of the substrates. In studies already performed by us [8–11], we managed to show the potential of such an approach when applied to systems of III–V semiconductor compounds (AlGaAs, GaInP, InGaAs, etc.).

However, in publications, there are no data on the optical properties of epitaxial GaAs layers grown on SL/proto-Si compliant substrates. Therefore, the purpose of this study is to conduct spectroscopic investigations of III–V/proto-Si/Si heterostructures and to compare the results with achievements in using the technology of growth on standard substrates.

2. EXPERIMENTAL

The structures to be studied were grown by metal–organic chemical vapor deposition (MOCVD) using an EMCORE GS3100 setup with a vertical reactor and

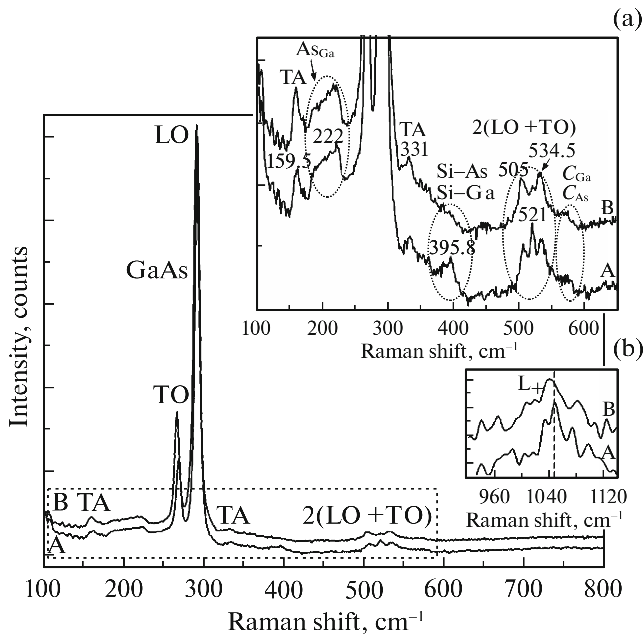

Fig. 1. Raman spectra of GaAs films grown on proto-Si(100) and SL/proto-Si(100) substrates. Insets: low-intensity vibrations in the Raman spectra of integrated heterostructures in the ranges (a) 100–650 and (b) 940–1030 cm^{-1}.

a resistively heated substrate holder. The pressure in the reactor was 77 Torr, and the speed of rotation of the substrate holder was 1000 rpm. The sources were trimethylgallium ($Ga(CH_3)_3$), trimethylaluminum ($Al(CH_3)_3$), and arsine (AsH_3). For the carrier gas, we used hydrogen (H_2). To grow the structure, we used Si(100) substrates misoriented by 3° with respect to the [110] direction.

The structures were grown by the technology described below.

In the first stage, a protoporous layer was formed on the surface of a Si wafer, similarly to how it was done in previous studies [5, 6]. The proto-Si layer was formed by 1-min etching of the initial wafer in a solution composed of one part hydrofluoric acid HF, one part acetic acid, and 40 parts nitric acid.

Then the treated Si wafer was annealed in AsH_3 at a temperature of 750°C for 20 min. Thereafter the temperature was lowered to 450°C for 7 min in the presence of an AsH_3 flux.

In the next stage, we grew a 10-nm-thick epitaxial AlAs layer and a 30-nm-thick GaAs layer, after which the temperature was elevated to 550°C for 7 min in the presence of an AsH_3 flux. At this temperature, a 360-nm-thick GaAs layer was grown to form structure A, and a ~100-nm-thick AlGaAs SL and a top 700-nm-thick GaAs layer were grown to form structure B.

To compare the results obtained in the study, we used a homoepitaxial GaAs/GaAs structure grown by the standard technology and studied by us previously [5]. This heterostructure was grown under the following conditions: the temperature of the substrate holder 700°C, the pressure in the reactor 77 Torr, and the speed of rotation of the substrate holder 1000 rpm. For the initial reagents, we used trimethylgallium ($Ga(CH_3)_3$) and arsine (AsH_3). The rate of growth of GaAs was ~770 Å min^{-1}.

The Raman spectra were recorded using a RamMix 532 confocal Raman microscope with a spectral resolution of 2 cm^{-1} in the range 200–2000 cm^{-1}. The spectra were excited with a laser emitting at the wavelength λ_{ex} = 532 nm; the radiation power on the sample was ~(10–50) mW. The signal was gathered with a 50× objective lens.

The photoluminescence (PL) spectra of the heterostructures were obtained for signals from the sample surfaces at room temperature by the standard procedure, using a TRIAX550 monochromator and a CCD detector cooled with liquid nitrogen. The PL signal was excited with an argon laser at an emission wavelength of 514.5 nm. The exposed area of the sample surface was 1 mm^2. To focus laser excitation on the surface, we used a 10× objective lens.

3. RESULTS AND DISCUSSION

3.1. Raman Spectroscopy

To study the structural features of epitaxially grown hybrid structures formed on compliant substrates of two types, we used Raman spectroscopy. The use of Raman scattering provides additional, new, and sometimes detailed data on the properties and crystal quality of layers in epitaxial heterostructures [12–14].

It is well known that gallium arsenide exhibits the zinc-blende structure, in which there are two different atoms per unit cell. In accordance with the Raman tensor, the spectrum of GaAs is bound to involve acoustic phonon modes (three types) and optical phonon modes (three types). In this case, the selection rules allow the manifestation of only longitudinal optical (LO) phonons for the (100) surface, transverse optical (TO) phonons for the (110) surface, and LO and TO phonons for the (111) surface [15]. However, for the chosen $z(xy)z$ geometric layout of measurements for a (100)-oriented zinc-blende-structured epitaxial layer, only LO phonons propagating along the normal to the (001) plane are allowed in the spectrum.

Figure 1 shows the experimental Raman spectra for heterostructures A and B grown on proto-Si and SL/proto-Si compliant substrates.

We can see that, in the spectra of the samples, the principal high-intensity reflection corresponds to the longitudinal LO_{Ga-As} vibration. In addition, forbidden

transverse TO_{Ga-As} phonons are evident in the spectra, which is indicative of some deviation of the orientation of the epitaxial layer from the [100] direction. Such a deviation arises from growth on a Si(100) substrate misoriented relative to the [110] direction. In more detail, the region of LO and TO phonons in the epitaxial GaAs layer is shown in Fig. 2. Figure 2 shows also the spectrum of homoepitaxial sample C grown by the standard technology. The lack of the TO mode in the spectrum of sample C is indicative of the ideal orientation of the epitaxial GaAs layer. In addition, it can be seen that the position of the longitudinal and transverse modes in the GaAs films grown on the compliant substrates is shifted from the position of the corresponding modes in the homoepitaxial structure, for which the phonon-mode frequencies exactly coincide with the frequencies known for the GaAs single crystal from publications [16]. The positions (ω) and full widths at half-maximum (FWHM) of the LO and TO phonon bands are indicated in Fig. 2. It should be noted that the observed asymmetry in the shape of the LO and TO vibrational bands for homoepitaxial sample C (Fig. 2) is due to plasmon–phonon interaction L_+ and L_-. As concerns the FWHM of the LO phonon band for samples A and B, we can state that it does not exceed 10 cm^{-1}, and this fact is indicative of the high crystal quality of the films grown in the study.

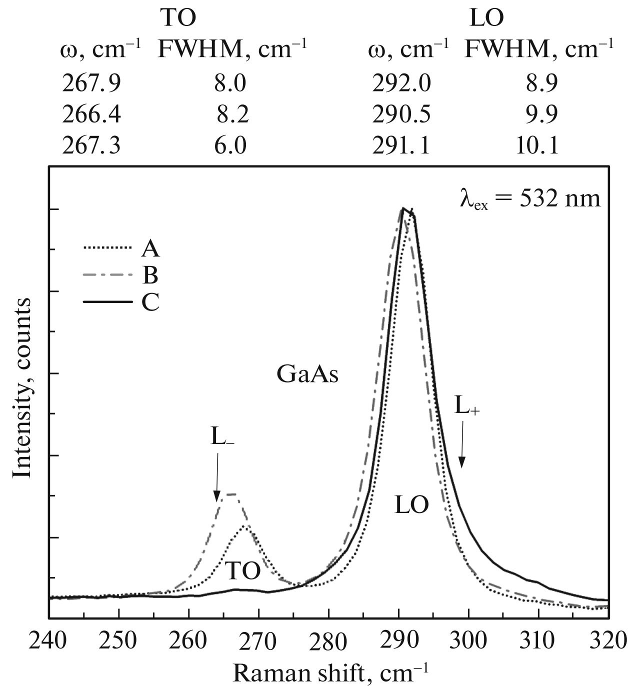

TO		LO	
ω, cm^{-1}	FWHM, cm^{-1}	ω, cm^{-1}	FWHM, cm^{-1}
267.9	8.0	292.0	8.9
266.4	8.2	290.5	9.9
267.3	6.0	291.1	10.1

Fig. 2. Region of LO and TO phonons in the Raman spectrum of the epitaxial GaAs layer in heterostructures A and B and homoepitaxial structure C.

Apart from the principal phonon modes, a number of low-intensity vibrations clearly seen in Figs. 1a and 1b are involved in the Raman spectra of both samples. In the spectra, we observe acoustic TA phonons near 160 and 330 cm^{-1} [17]. The low-intensity structure between 500 and 530 cm^{-1} is defined by second-order phonon scattering [18]. The observed slight differences between the spectra in this range are defined by shifts in the geometric layout of scattering.

The vibration localized near 390 cm^{-1} can be associated with the incorporation of Si atoms into the GaAs lattice; as a consequence, the local Si–Ga or Si–As modes can appear in the Raman spectrum at 390 cm^{-1} [19]. It can be clearly seen that vibration in this region is observed only in the spectrum of heterostructure A. The SL introduced into the composition of the compliant substrate protects the epitaxial layer from self-doping with Si atoms that diffuse from the substrate.

MOCVD growth at reduced temperatures promotes self-doping of the epitaxial layer with carbon atoms during growth [14], and therefore, carbon lines can be observed in the spectra. According to the data of [20], carbon-related lines in the Raman spectra are bound to be observed near 580 cm^{-1}. As can be seen from the experimental data (see Fig. 1a), a slight scattering response is observed in this region of the spectra of heterostructures A and B, which is indicative of a low content of carbon incorporated into the GaAs crystal lattice during growth.

The broad line observed in the Raman spectra in the range 200–230 cm^{-1} is a consequence of the low-temperature growth of GaAs films and is associated with an excess content of As and accompanying point defects, such as As_{Ga} antisite defects and Ga vacancies [15].

One more feature of the spectra of heterostructures grown on compliant substrates is the mode observed in the region of 1040 cm^{-1} (see Fig. 1b). According to the data reported in [18, 21], this vibration is a plasmon-like mode L_+ of the *n*-GaAs layer, with an intensity dependent on the concentration of free charge carriers. It should be noted that, in [18], the vibration intensity in this spectral region relative to the LO-mode intensity in GaAs was much higher that the intensity observed in the spectra here. In that case, the concentration of charge carriers in [18] was at a level of $\sim 10^{19}$ cm^{-3}.

As repeatedly shown, Raman spectroscopy is a sensitive tool for measuring stresses in epitaxial layers. The origin of stresses can be thermal, i.e., defined by different expansion coefficients of the constituent materials of the heteropair or by temperature gradients during growth of the sample. However, the main cause of stresses is the difference between the lattice parameters of the materials.

The stresses in the layer can be analyzed using data on the shift of the TO/LO phonon mode. In this case,

Table 1. Results of Raman spectroscopy

Structure	$\Delta\omega_0$, cm^{-1}	σ, MPa
A	0.9	212
B	–0.6	141

the shift is positive under compressive stresses in the layer and negative under tensile stresses.

These stresses present a serious problem for device operation, since they can induce the formation of defects, such as dislocations responsible for cracking and for reducing the service life of the device.

Since only LO phonons are allowed in the Raman spectrum of epitaxial semiconductor layers with a cubic lattice and (001) orientation of the surface, the residual stresses in the crystal lattice can be estimated from the Raman shift of the LO phonon band.

In accordance with the data of [21], the Raman shift $\Delta\omega_0$ defined by stresses can be determined from the relation

$$\Delta\omega_0 = \frac{1}{\omega_0}[S_{11}p + (S_{12} + S_{11})q]\sigma. \quad (1)$$

Here, S_{ij} are the elastic compliance coefficients, p and q are the constants that show how the elastic compliance coefficients vary under the action of stresses, and σ is the mechanical stress.

The relations between the Raman shift $\Delta\omega_0$ and the stress σ in the GaAs crystal were determined experimentally depending on the type of the heterojunction [22]. For the GaAs/Si heterojunction in the case of the biaxial stress σ (in GPa) in the (100) plane, the relation

$$\Delta\omega_0 = 4.24\sigma \quad (2)$$

holds well for the Raman shift (in cm^{-1}).

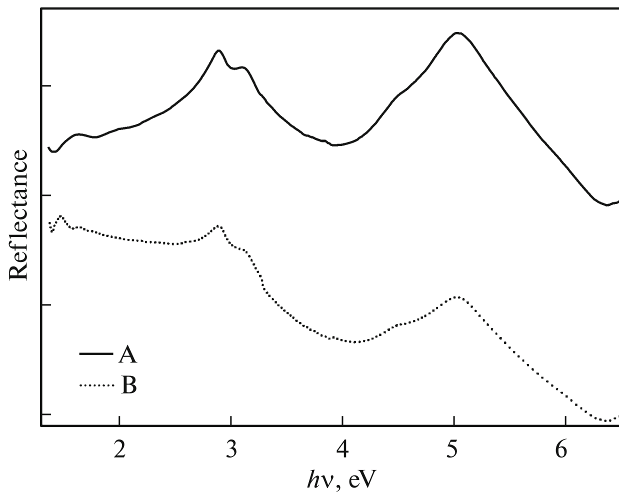

Fig. 3. Experimental transmittance–reflectance spectra at the angle of incidence of radiation 8° for heterostructures grown on the proto-Si(100) and SL/proto-Si(100) substrates.

In the epitaxial GaAs layers grown on compliant substrates, the shifts of the LO and TO phonon bands (see Fig. 2) with respect to the position of these vibrational bands in the homoepitaxial structure are given in Table 1. It can be noted that, in accordance with the direction of the shift $\Delta\omega_0$, the epitaxial GaAs layer in heterostructure A experiences compressive stresses, whereas the negative shift $\Delta\omega_0$ for heterostructure B suggests the appearance of tensile stresses. These results are in agreement with the X-ray diffraction data, from which the crystal-lattice parameter of the epitaxial GaAs film was determined with consideration for internal stresses (a^v).

Using relation (2), we calculated the stresses σ for heterostructures A and B (Table 1).

It can be clearly seen that the stress in the epitaxial GaAs layer of the heterostructure grown on the SL/proto-Si substrate is almost 50% lower than that in the heterostructure formed on the proto-Si substrate.

It should be noted that the level of stresses determined from the Raman data corresponds to the stresses in the upper layers of the epitaxial GaAs film, since the effective depth of scattering is ~100 nm.

3.2. Optical Spectroscopy

The optical properties of heterostructures in the ultraviolet and visible regions were studied on the basis of the approach repeatedly used by us in previous studies. We here used the reflection-recording procedure tested by us in a series of earlier studies [23–26]. This approach provides a means for studying the fundamental optical properties of epitaxial films grown on different substrates.

To follow this approach, we recorded the transmittance–reflectance spectra of GaAs/Si heterostructures in the wavelength range 190–900 nm at nearly normal incidence of electromagnetic radiation. The experimental transmittance–reflectance spectra are shown in Fig. 3. As can be clearly seen from Fig. 3, the spectra exhibit a number of characteristic features. In accordance with fundamental concepts [27], the peaks in the transmittance–reflectance spectra of the samples correspond to transitions at the points Γ, L, and Λ in GaAs; in this case, the transitions at points L, and Λ give doublets because of spin–orbit splitting of the valence band.

To clarify the features of the mechanisms of optical absorption in the epitaxial GaAs layer on the basis of the Lambert–Bouguer formula

$$T = \exp[-D], \quad (3)$$

and the Kramers–Kronig relations [28], we transformed the transmittance–reflectance spectra into absorption spectra. Here, T is the transmittance and D is the optical density. Then we constructed the dependence of the quantity $(Dh\nu)^2$ on the photon energy $h\nu$ (Fig. 4).

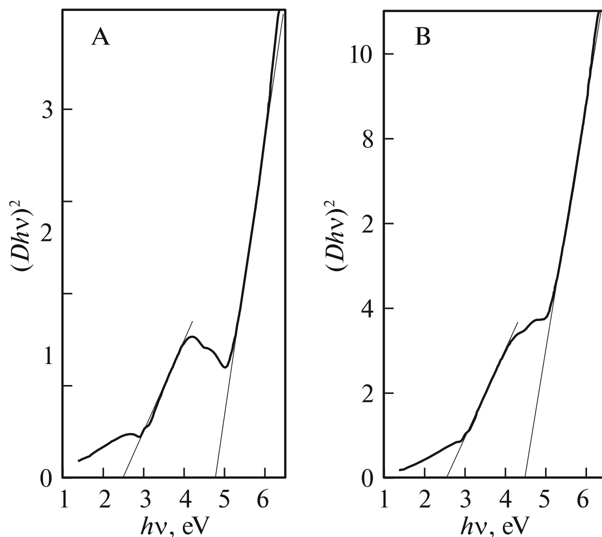

Fig. 4. Dependences of the quantity $(Dh\nu)^2$ on the photon energy $h\nu$ for the integrated heterostructure samples GaAs/proto-Si(100) (sample A) and GaAs/SL/proto-Si(100) (sample B).

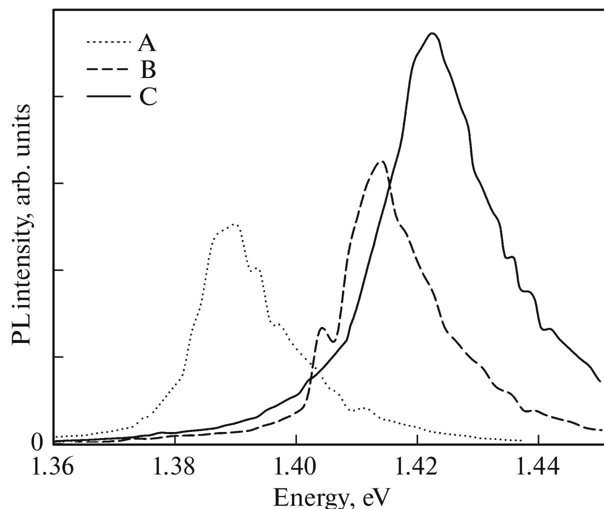

Fig. 5. PL spectra of heterostructures A and B and homoepitaxial structure C at room temperature.

Graphical analysis of this dependence makes it possible to separate out linear portions in it (Fig. 4). From linear extrapolation of these portions to zero, it is possible to determine the energies of direct transitions characteristic of the samples.

Table 2 lists the energies determined by the above-described procedure for the direct transitions and features observed in the spectra of the samples. Table 2 also gives the previously reported data for single-crystal GaAs [27].

As concerns the features in the spectra of integrated GaAs/Si heterostructures, it should be noted that the energy position of the features practically coincides with the corresponding data for single-crystal GaAs. However, it should be noted that, in the spectrum of GaAs grown on compliant substrates, we can see a shift to higher energies for direct transitions at the point Γ and a shift to lower energies at the point L. In this case, with increasing residual stresses, the shift increases. When comparing the results obtained here and the data of our previous study, wherein we investigated a homoepitaxial GaAs/GaAs structure (sample C) and established the effect of misorientation of the substrate and its preliminary etching on the optical properties, we can see direct correlation of the data. In this case, the SL introduced into the composition of the compliant substrate has a positive effect on the optical characteristics of the epitaxial film, which is manifested by smaller energy shifts of allowed direct transitions.

3.3. PL Studies

The crystal quality of the epitaxial GaAs layer and the deviation from the stoichiometric ratio upon growth on a compliant substrate with a SL are necessarily bound to influence the PL signal, i.e., the energy characteristics of the samples.

The PL spectra of two heterostructure samples and homoepitaxial heterostructure sample C are shown in Fig. 5. As follows from the experimental data, the epitaxial GaAs layers grown on the proto-Si and SL/proto-Si compliant substrates exhibit a single-mode structure of the PL spectrum. The line is in the energy range 1.47–1.5 eV and corresponds to radiative band-to-band transitions that coincide in energy with the band gap of GaAs. The PL intensity and the position of the PL band in the spectrum depend on the type of the sample. The maximum PL intensity is inherent in homoepitaxial sample C. The shift of the

Table 2. Results of analysis of the optical spectra of heterostructure samples

Sample	Energies of direct transitions and spectral features (in eV) and their identification in accordance with the data of [27]				
	Λ3–Λ1		L3–L1	Γ15–Γ15	X5–X1
A	2.9	3.13	2.48	4.78	5.03
B	2.88	3.10	2.58	4.50	5.03
GaAs [27]	2.90	3.14	2.6	4.2	5.12

peak of the PL bands for heterostructures A and B with respect to the peak for homoepitaxial structure C is defined by stresses in the crystal lattice and correlates with the elastic stresses observed in the epitaxial GaAs layer (Table 2).

4. CONCLUSIONS

The experimental results obtained in the study show that the introduction of a SL into the composition of the compliant substrate makes it possible to mitigate a number of negative effects of low-temperature growth, to redistribute stresses produced in the crystal lattice, and to reduce the number of technological operations of growth of transition buffer layers.

According to the Raman spectroscopy data, the stresses induced in the epitaxial GaAs layer by the mismatch between the crystal lattices in the case of the heterostructure grown on the SL/proto-Si compliant substrate are almost 50% smaller than the stresses in the heterostructure formed on the proto-Si substrate. The shift of the peak of the PL band in the heterostructures is defined by stresses in the crystal lattice and correlates with the elastic stresses observed in the epitaxial GaAs layer.

The introduction of a SL into the composition of the compliant substrate has a positive effect on the optical properties of the epitaxial film, which is manifested by the smaller energy shifts of allowed direct transitions.

The data obtained in the study will serve as an important material for understanding the fundamentals of the physics and technology of integrated III–V/Si heterostructures and for promoting their potential for use in optoelectronic devices.

ACKNOWLEDGMENTS

We thank the Karlsruhe Nano Micro Facility (KNMF, www.kit.edu/knmf) of the Forschungszentrum Karlsruhe for providing access to equipment at their laboratories.

FUNDING

The study was supported by the Russian Science Foundation, project no. 19-72-10007.

The part of the study performed by P.V. Seredin was supported by the Ministry of Science and Higher Education of the Russian Federation, project no. FZGU-2020-0036, in accordance with the government order to institutes of higher education.

The technological studies of epitaxial MOCVD processes were conducted in accordance with the planned state program of the Ioffe Institute.

CONFLICT OF INTEREST

The authors declare that they have no conflict of interest.

REFERENCES

1. A. Ballabio, S. Bietti, A. Scaccabarozzi, L. Esposito, S. Vichi, A. Fedorov, A. Vinattieri, C. Mannucci, F. Biccari, A. Nemcsis, L. Toth, L. Miglio, M. Gurioli, G. Isella, and S. Sanguinetti, Sci. Rep. **9** (2019). https://doi.org/10.1038/s41598-019-53949-x
2. M. Feifel, D. Lackner, J. Ohlmann, J. Benick, M. Hermle, and F. Dimroth, Sol. RRL **3**, 1900313 (2019). https://doi.org/10.1002/solr.201900313
3. A. A. Geldash, V. N. Djuplin, V. S. Klimin, M. S. Solodovnik, and O. A. Ageev, J. Phys.: Conf. Ser. **1410**, 012030 (2019). https://doi.org/10.1088/1742-6596/1410/1/012030
4. P. V. Seredin, D. L. Goloshchapov, A. S. Lenshin, A. M. Mizerov, and D. S. Zolotukhin, Phys. E (Amsterdam, Neth.) 104, 101 (2018). https://doi.org/10.1016/j.physe.2018.07.024
5. P. V. Seredin, A. S. Lenshin, D. S. Zolotukhin, I. N. Arsentyev, A. V. Zhabotinskiy, and D. N. Nikolaev, Phys. E (Amsterdam, Neth.) 97, 218 (2018). https://doi.org/10.1016/j.physe.2017.11.018
6. P. V. Seredin, A. S. Lenshin, D. S. Zolotukhin, I. N. Arsentyev, D. N. Nikolaev, and A. V. Zhabotinskiy, Phys. B (Amsterdam, Neth.) **530**, 30 (2018). https://doi.org/10.1016/j.physb.2017.11.028
7. P. V. Seredin, A. S. Lenshin, A. M. Mizerov, H. Leiste, and M. Rinke, Appl. Surf. Sci. **476**, 1049 (2019). https://doi.org/10.1016/j.apsusc.2019.01.239
8. P. V. Seredin, A. V. Glotov, E. P. Domashevskaya, I. N. Arsentyev, D. A. Vinokurov, and I. S. Tarasov, Appl. Surf. Sci. **267**, 181 (2013). https://doi.org/10.1016/j.apsusc.2012.09.053
9. E. P. Domashevskaya, P. V. Seredin, A. N. Lukin, L. A. Bityutskaya, M. V. Grechkina, I. N. Arsentyev, D. A. Vinokurov, and I. S. Tarasov, Surf. Interface Anal. **38**, 828 (2006). https://doi.org/10.1002/sia.2306
10. P. V. Seredin, D. L. Goloshchapov, Yu. Yu. Khudyakov, A. S. Lenshin, A. N. Lukin, I. N. Arsentyev, and T. Prutskij, Phys. B (Amsterdam, Neth.) **509**, 1 (2017). https://doi.org/10.1016/j.physb.2016.12.030
11. T. Prutskij, P. Seredin, and G. Attolini, J. Lumin. **195**, 334 (2018). https://doi.org/10.1016/j.jlumin.2017.11.016
12. P. V. Seredin, A. S. Lenshin, A. V. Glotov, I. N. Arsentyev, D. A. Vinokurov, I. S. Tarasov, T. Prutskij, H. Leiste, and M. Rinke, Semiconductors **48**, 1094 (2014). https://doi.org/10.1134/S1063782614080211
13. P. Seredin, A. Glotov, E. Domashevskaya, I. Arsentyev, D. Vinokurov, A. Stankevich, and I. Tarasov, in *Advanced Materials and Technologies for Micro/Nano-Devices, Sensors and Actuators*, Ed. by E. Gusev, E. Garfunkel, and A. Dideikin (Springer, Netherlands, Dordrecht, 2010), p. 225.
14. P. V. Seredin, A. V. Glotov, E. P. Domashevskaya, I. N. Arsentyev, D. A. Vinokurov, and I. S. Tarasov, Phys. B (Amsterdam, Neth.) **405**, 2694 (2010). https://doi.org/10.1016/j.physb.2010.03.049

15. D.-S. Jiang, X.-P. Li, B.-Q. Sun, and H.-X. Han, J. Phys. D: Appl. Phys. **32**, 629 (1999). https://doi.org/10.1088/0022-3727/32/6/005
16. *Properties of Semiconductor Alloys: Group-IV, III–V and II–VI Semiconductors*, Ed. by Sadao Adachi (Wiley, Chichester, UK, 2009).
17. N. M. Belyi, O. V. Vakulenko, V. A. Gubanov, and V. A. Skryshevskii, J. Appl. Spectrosc. **41**, 938 (1984). https://doi.org/10.1007/BF00659848
18. W. Q. Li, P. K. Bhattacharya, S. H. Kwok, and R. Merlin, J. Appl. Phys. **72**, 3129 (1992). https://doi.org/10.1063/1.351474
19. A. G. Rodríguez, H. Navarro-Contreras, and M. A. Vidal, J. Appl. Phys. **90**, 4977 (2001). https://doi.org/10.1063/1.1410886
20. B. Pajot, B. Clerjaud, and B. Pajot, *Electronic Absorption of Deep Centres and Vibrational Spectra* (Springer, Heidelberg, 2013).
21. S. Perkowitz, *Optical Characterization of Semiconductors: Infrared, Raman, and Photoluminescence Spectroscopy* (Academic, London, San Diego, 1993).
22. J. Jimenez and J. W. Tomm, *Spectroscopic Analysis of Optoelectronic Semiconductors* (Springer, Cham, 2016).
23. V. A. Volodin, M. D. Efremov, V. Ya. Prints, V. V. Preobrazhenskii, B. R. Semyagin, and A. O. Govorov, J. Exp. Theor. Phys. Lett. **66**, 47 (1997). https://doi.org/10.1134/1.567481
24. P. V. Seredin, A. S. Lenshin, V. M. Kashkarov, A. N. Lukin, I. N. Arsentiev, A. D. Bondarev, and I. S. Tarasov, Mater. Sci. Semicond. Process. **39**, 551 (2015). https://doi.org/10.1016/j.mssp.2015.05.067
25. P. V. Seredin, V. M. Kashkarov, I. N. Arsentyev, A. D. Bondarev, and I. S. Tarasov, Phys. B (Amsterdam, Neth.) **495**, 54 (2016). https://doi.org/10.1016/j.physb.2016.04.044
26. P. V. Seredin, A. S. Lenshin, D. L. Goloshchapov, A. N. Lukin, I. N. Arsentyev, A. D. Bondarev, and I. S. Tarasov, Semiconductors **49**, 915 (2015). https://doi.org/10.1134/S1063782615070210
27. J. Tauc, Prog. Semicond. **9**, 87 (1965).
28. Yu. I. Ukhanov, *Optical Properties of Semiconductors* (Nauka, Moscow, 1977) [in Russian].

Translated by E. Smorgonskaya